Chemically Controlled Reversible and Irreversible Extraction Barriers Via Stable Interface Modification of Zinc Oxide Electron Collection Layer in Polycarbazole-based Organic Solar Cells

*Sarah R. Cowan, Philip Schulz, Anthony J. Giordano, Andres Garcia, Bradley A. MacLeod, Seth R. Marder, Antoine Kahn, David S. Ginley, Erin L. Ratcliff, and Dana C. Olson**

A spin-cast method is presented for the formation of phosphonic acid functionalized small molecule layers on solution-processed ZnO substrates for use as electron collecting interlayers in organic photovoltaics. Phosphonic acid interlayers modify the ZnO work function and the charge carrier injection barrier at its interface, resulting in systematic control of V_{OC} in inverted bulk heterojunction solar cells. Surface modification is shown to moderate the need for UV light-soaking of the ZnO contact layers. Lifetime studies (30 days) indicate stable and improved OPV performance over the unmodified ZnO contact, which show significant increases in charge extraction barriers and series resistance. Results suggest that enhanced stability using small molecule modifiers is due to partial passivation of the oxide surface to molecular oxygen adsorption. Surface passivation while maintaining work function control of a selective interlayer can be employed to improve net efficiency and lifetime of organic photovoltaic devices. The modified cathode work function modulates V_{OC} via static energetic barriers and modulates contact conductivity by creating reversible and irreversible S-shape current-voltage characteristics as a result of kinetic barriers to charge transport.

1. Introduction

Investment in photovoltaic technologies over the past 5–10 years has enabled organic photovoltaic research and development to transition from primary focus on laboratory research toward enabling the first viable industrial products. Research and development is motivated, in part, by reports of single module devices with reported power conversion efficiencies in the range of 10–12%,[1–3] and regularly reported laboratory power conversion efficiencies from 7–9%.[4–8] New materials and device architectures rely less upon traditional contacts utilized in the field for more than a decade—PEDOT:PSS and calcium/aluminum—but increasingly employ metal oxide contacts, often solution-processed from sol-gel precursors or nanoparticles. Metal oxides, when used as contact interlayers in bulk heterojunction polymer and small molecule solar cells, have been shown to either i) eliminate the fast degradation processes caused by the unstable high-electron affinity metals[9,10] and/or acidic PEDOT:PSS-based materials;[11] or ii) prolong the lifetime of the bulk heterojunction (BHJ) device by acting as oxygen- and/or water-getters and barriers to diffusion of atmospheric constituents into devices, thereby extending the usable life span of these devices by orders of magnitude—from minutes to months or years.[11]

Zinc oxide (ZnO) is a promising candidate for contact layers in next-generation thin-film photovoltaics because it is a low-cost, non-toxic, earth-abundant material with multiple solution deposition routes to the formation of thin films. However, in multiple studies, zinc oxide and other metal oxides have demonstrated a dependence of work function and conductivity on UV light-soaking when exposed to air.[12–16] In polymer : fullerene BHJ photovoltaics, the ZnO contact layer has been shown to affect the diode properties of the device and result in the formation of an S-kink, though full initial performance can be regained through UV light-soaking.[4]

In addition to light-soaking effects, previous research has shown that ZnO is easily etched via a number of simple solvents and in mild acidic conditions.[17] The chemical dissolution of the stoichiometric oxide leads to a complex surface of hydroxyls and physisorbed or chemisorbed species (including O_2, CO, CO_2, and H_2); these changes in near-surface composition are strongly linked to both the electronic structure and the semiconducting properties desired for oxide inclusion in

Dr. S. R. Cowan, Dr. A. Garcia, Dr. B. A. MacLeod, Dr. D. S. Ginley, Dr. D. C. Olson
National Center for Photovoltaics
National Renewable Energy Laboratory
Golden, CO 80401, USA
E-mail: Dana.Olson@nrel.gov
Dr. P. Schulz, Prof. A. Kahn
Department of Electrical Engineering
Princeton University
Princeton, NJ 08544, USA
Dr. A. J. Giordano, Prof. S. R. Marder
School of Chemistry and Biochemistry
and Center for Organic Photonics and Electronics
Georgia Institute of Technology
Atlanta, GA 30332–0400, USA
Prof. E. L. Ratcliff
Department of Chemistry
University of Arizona
Tucson, AZ 85721, USA

DOI: 10.1002/adfm.201400158

electronic devices.[18–22] Likewise, the degree of crystallinity, exposed crystal face, sol-gel precursor, thermal treatment, and film surface roughness will all play an important role in determining both the initial structure-function relationships of the ZnO thin films as well as the temporal chemical resistance to change over the lifetime of the device. For example, in all but three cases, work function modification of ZnO has shown little longevity due to poor chemical resistance to ambient environments.[12,23,24] Previous studies have demonstrated work function modification of transparent conducting oxides (TCOs) via monolayer deposition of benzyl phosphonic acid,[25,26] and shown a correlation between work function modification and open circuit voltage in solar cell device structures.[12,26] Benzyl phosphonic acids (BPAs) have been demonstrated to modify the work function of indium tin oxide (ITO) in the absence of selective interlayers, like ZnO, nickel oxide (NiO), molybdenum oxide (MoO_3), or titanium suboxide (TiO_x) for efficient extraction of photogenerated charges. However BPA-modified ITO contacts are notably poor at blocking charge injection in reverse bias (i.e. low shunt resistance),[26] a situation that is greatly improved when a charge selective oxide interlayer is used between the TCO and the BHJ.

An attractive solution is to combine small molecule modifiers for work function control and defect passivation with the selective oxide contacts.[27] However, previous work has been carried out using deposition methods, which expose the oxide to excess solvent—dip coating or substrate soaking for one to many days in a dilute solution. Initial attempts to deposit benzyl phosphonic acids or carboxylic acids via dip coating or spin coating on thick ZnO films have been shown to etch ZnO under certain conditions.[28]

The present study investigates the effects of modulation of the ZnO work function through spin-cast layers of dipolar benzyl phosphonic acids (BPA) on device performance and stability. Also investigated is the effect of the BPA on the light-soaking characteristics of inverted poly[*N*-9′-heptadecanyl-2,7-carbazole-alt-5,5-(4′,7′-di-2-thienyl-2′,1′,3′-benzothiadiazole)] (PCDTBT): (6,6)-phenyl C_{71}-butyric acid methyl ester ($PC_{71}BM$) BHJ solar cells with ZnO films formed from a diethylzinc precursor. In this work, we demonstrate that the use of a series of interfacial modifiers leads to both work function modification of the ZnO interface, and a proportional change in the open circuit voltage in BHJ solar cells. However, unlike traditionally used methods of soaking the substrate in a solution of modifier, a spin-casting method employed here decreases exposure time of the ZnO to the acidic solution, allowing non-destructive modification of the ZnO thin films. The deposition of BPAs is shown here to have no detrimental impact on the lifetime of devices over the testing period of 30 days storage in air. The inherent surface properties (chemical and electronic) of the unmodified and modified ZnO thin films are characterized using X-ray photoelectron spectroscopy (XPS), ultraviolet photoelectron spectroscopy (UPS), inverse photoemission spectroscopy (IPES), and Kelvin probe studies. In an extended aging test of the thin films, we investigate the effect of prolonged exposure to ambient conditions on the work function via Kelvin probe. We construct full inverted polymer : fullerene BHJ devices with the following structures, glass/ITO/ZnO/PCDTBT:$PC_{71}BM$/MoO_3/Ag, and glass/ITO/ZnO/modifier/PCDTBT:$PC_{71}BM$/MoO_3/Ag, and compare the effects of modifying the ZnO surface on device characteristics as-prepared and after 30 days aging in air. We look in detail at the dependence of device characteristics on the net UV exposure from incident illumination by a filtered solar simulator and show that the reversible aging effect on ZnO can be partially mitigated via the introduction of interfacial dipole modifiers between the ZnO and BHJ layers.[29] Furthermore, we present evidence that suggests that this mitigation effect is not limited to the ZnO interface, but also affects the bulk conductivity of the ZnO electron transport layer (ETL). These results indicate that a detailed understanding of both modifier attachment group as well as deposition method is necessary when using amphoteric oxides in organic photovoltaics.

2. Electronic Structure of BPAs on ZnO Deposited from Diethylzinc

The electronic structure of ZnO deposited from diethylzinc sol-gel and ZnO modified with the phosphonic acids pCF_3BPA and oF_2BPA, as probed via ultraviolet photoelectron spectroscopy (UPS) and inverse photoemission spectroscopy (IPES), is presented in **Figure 1**. UPS is used to determine the position of the vacuum level (E_{vac}), the surface work function (WF), and the ionization energy (IE) of the material, whereas IPES is used to measure the electron affinity (EA). E_{vac} is determined from the onset of the secondary electron peak shown on the left panels of Figure 1. The WF is then the energy difference between E_{vac} and the Fermi level (E_F). Likewise, the position of the onset of the density of occupied states with respect to E_{vac} is a measure of IE, while the position of the unoccupied states, measured by IPES with respect to E_{vac}, is the EA of the surface. Successful deposition of the benzyl phosphonic acids, oF_2BPA and pCF_3BPA, on ZnO is confirmed by XPS in Figure S1 (Supporting Information).

The bare ZnO surface exhibits a fairly low WF of 3.6 eV. The joint UPS/IPES analysis reveals the n-type nature of the ZnO, with the onset of unoccupied states present at 0.8 eV above the Fermi level. The valence band onset is very deep with tail states ranging up to 3.1 eV below E_F, yielding an electronic gap of 3.9 eV for the ZnO surface.

The WF of the ZnO/BPA contact shifts according to BPA dipole strength, as observed in previous studies.[25] Given that we cannot rule out the possibility of multilayers (as films are spin-cast and not self-assembled), this result suggests that WF control via phosphonic acids may not be entirely orientation dependent, as supported by data in Figure S2a (Supporting Information), which compares BPA WF modification by deposition method (soaking and spin-casting). The WF of ZnO modified with pCF_3BPA increases by 0.9 eV deeper (4.5 eV) with respect to pristine ZnO (3.6 eV), as shown by the vacuum level shift in the far left panel of Figure 1c. Conversely, the WF of ZnO modified with oF_2BPA decreases by 0.2 eV (3.4 eV) compared to pristine ZnO (Figure 1e). The trend in WF agrees with the dipole strength and direction of the molecules, as determined by orientation of the polarizing fluorine molecule position on the benzene ring (molecular dipole).[25] Also, in

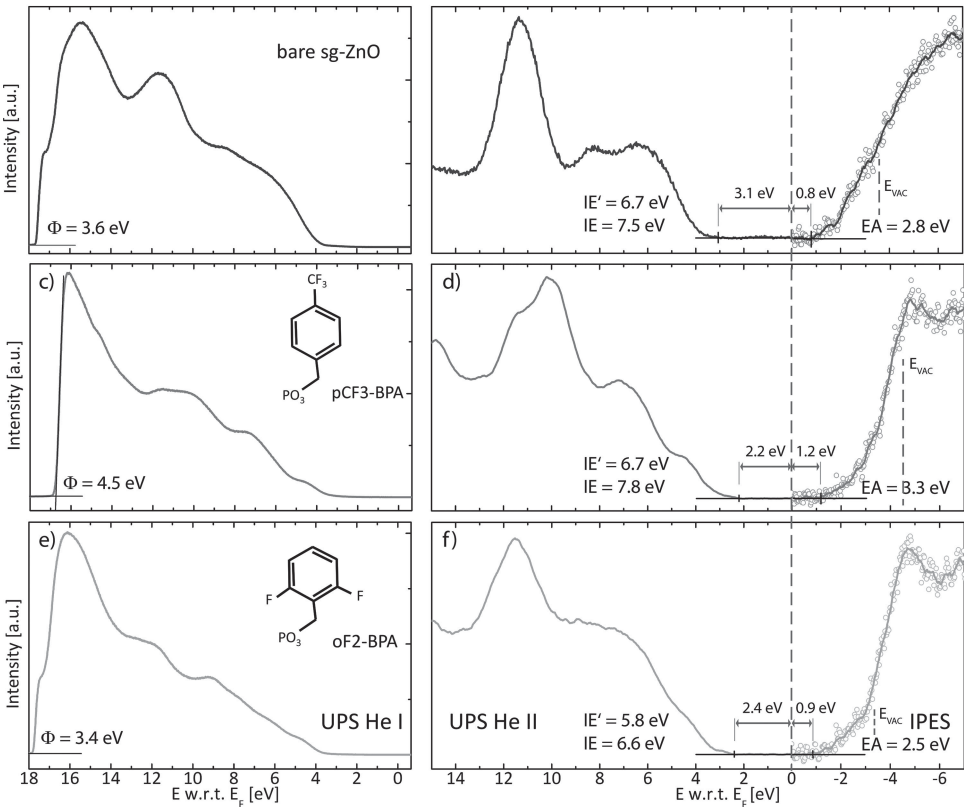

Figure 1. Ultraviolet photoelectron spectroscopic (UPS)/inverse photoemission spectra (IPES) of a,b) pristine ZnO, and ZnO modified by spin-cast layers of phosphonic acids, c,d) pCF_3BPA, and e,f) oF_2BPA. (c-f) show the electronically modified interface in the presence of the spin-cast benzyl phosphonic acid (pCF_3BPA and oF_2BPA), namely the WF shift and band offsets of the modified ZnO surface.

the absence of UV light, WF modification is shown via Kelvin probe to be possible over a range of 1.6 V contact potential difference (Figure S2b, Supporting Information) via a range of BPA molecules: ortho-difluorobenzyl phosphonic acid (oF_2BPA), benzyl phosphonic acid (BPA), pentafluoro benzyl phosphonic acid (pFBPA), and para-trifluoro benzyl phosphonic acid (pCF_3BPA).

In addition to producing WF changes, the BPA modifiers were observed to narrow the electrical band gap at the surface of ZnO. UPS/IPES measurements of the electronic structure shows that this narrowing is primarily due to the introduction of states near the ZnO valence band edge (≈0.7 eV). In the pCF_3BPA case, this narrowing is also accompanied by a downward shift of the Fermi level in the gap, indicating the ZnO is less apparently n-type, at least near the surface. However, the effect is partially compensated by a shift of the conduction band minimum by approximately 0.4 eV away from the Fermi level. In case of oF_2BPA the shift of the conduction band is less pronounced (0.1 eV). In addition to the narrowed band gap in particular, the pCF_3BPA-covered ZnO film shows significantly less n-type behavior. The introduction of the sub-gap states in the valence band may play a role in the more significant recovery of the BPA-modified ZnO films under lower energy illumination, as compared to their unmodified ZnO counterparts, as discussed below.

3. Chemical Modification of the ZnO Contact in As-Prepared and Aged Polymer BHJ Solar Cells

The electronic properties of pristine thin film ZnO and ZnO modified with benzyl phosphonic acids are directly applicable to polymer : fullerene bulk heterojunction devices incorporating the thin films as contacts. Inverted bulk heterojunction devices with the structure: glass/ITO/ZnO/modifier (optional)/PCDTBT:$PC_{71}BM$ BHJ/MoO_3/Ag were fabricated as specified in the Experimental Section.

The current density–voltage (*J–V*) characteristics of these devices, illuminated under 1 sun intensity and tested in an inert environment after incidental air exposure during device fabrication, are plotted in **Figure 2**. Four device types are intensively tested—glass/ITO/ZnO/modifier (optional)/PCDTBT:$PC_{71}BM$ BHJ/MoO_3/Ag, where one control device type (ZnO pristine) has no modifier applied and another control device type (ZnO/EtOH) has anhydrous ethanol spin-cast onto the annealed ZnO film under the same conditions as for the soluble modifier deposition.

The importance of the change in the work function of the modified ZnO surface in conjunction to the adjacent BHJ can be seen in the band diagram in **Figure 3**, derived from UPS measurements of thin BHJ films spin-cast on modified ZnO films presented in Figure S3 (Supporting Information). The

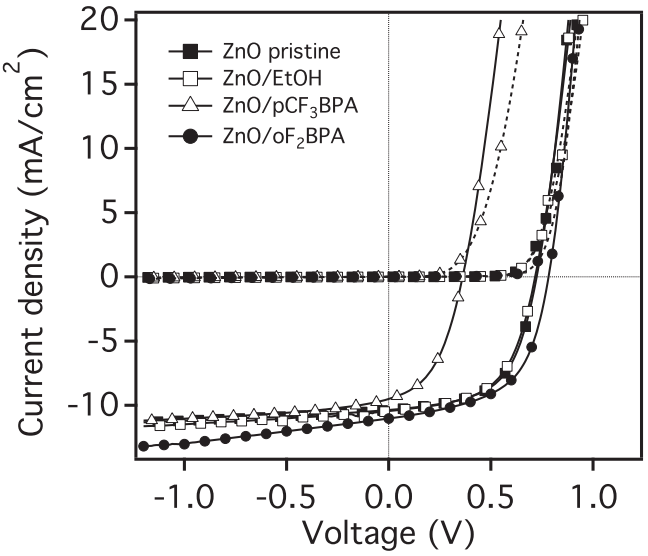

Figure 2. Device characteristics for inverted architecture PCDTBT:$PC_{71}BM$ solar cells using the benzyl phosphonic acids as contact modifiers on the ZnO electron transport layer as-fabricated, with pristine ZnO (black squares), ZnO treated with ethanol (white squares), pCF_3BPA-modified ZnO (white triangles), and oF_2BPA-modified ZnO (black circles) ETL contact. Lines are guides to the eye.

electronic gap of the PCDTBT:$PC_{71}BM$ thin films was previously measured using UPS/IPES.[32] This gap is used here to determine the position of the lowest unoccupied molecular orbital (LUMO) of the BHJ acceptor relative to the onset of the highest occupied molecular orbital (HOMO) of the donor.

As seen in Figure 3, each interface between the BHJ and the ZnO film present statistically significant differences in the position of the BHJ HOMO and LUMO with respect to the Fermi level of the ZnO film. Given the complexity of the evaluation of the energetics at the buried interface, we cannot rule out an interfacial dipole (occurring within 1–2 nm of the interface) versus a longer-range electronic effect.

For the BHJ on the unmodified ZnO surface (Figure 3a), there is a 0.5 eV shift in the vacuum level at the interface, resulting in a BHJ work function of 4.1 eV. The onset of occupied states in the BHJ is at 1.1 eV below the Fermi level, corresponding to an ionization energy (IE) of the blend of 5.2 eV. Using an electronic gap of 1.5 eV, we estimate the onset of unoccupied states approximately at 0.4 eV above the Fermi level, corresponding to an electron affinity (EA) of 3.7 eV. From Figure 1, the onset of unoccupied states in the ZnO film is at 0.8 eV above the Fermi level. Hence, an electron in the LUMO of the fullerene must overcome a 0.4 eV barrier to be injected into the ZnO. Part of this barrier may be compensated at the buried interface or via spatial effects in the operating device, as we do not observe an S-shape in the device performance in Figure 2.

Increasing the work function of the underlying ZnO by 0.9 eV with the pCF_3BPA interfacial modifier considerably increases the ZnO WF and lowers the Fermi level in the gap at the surface of the oxide. At the interface with the BHJ, a small interface dipole lowers the BHJ vacuum level with respect to that of the oxide. The result of these shifts is that the fullerene LUMO is now 0.6 eV below the onset of ZnO unoccupied states, that is, a larger barrier for electrons to overcome upon extraction. This offset makes the pCF_3BPA-modified ZnO contact less suitable to electron extraction from $PC_{71}BM$ in the BHJ due to a static energetic mismatch across the ZnO/$PC_{71}BM$ interface.

Conversely, the energetic picture in Figure 3(c) suggests a more favorable molecular level alignment between the BHJ and the oF2BPA-modified ZnO. As in the case with the unmodified ZnO, there is an upward shift in the vacuum level of the blend relative to that of the oxide surface. The onset of the occupied and unoccupied density of states of the BHJ are found at about 0.9 eV below and 0.6 eV above the Fermi level, respectively. Given the Fermi level position at the surface of the modified ZnO, the barrier to extraction is reduced to 0.3 eV.

The energy diagrams derived from spectroscopy (Figure 3) correlate well with device behaviors (Figure 2). The increases in the extraction barrier in the pCF_3BPA case correlates with a strong reduction in open circuit voltage without a large reduction in J_{sc} or FF, likely due to increased recombination at the electron contact caused in part by poor electron extraction efficiency. Conversely, evidence of a more favorable energy level alignment for electron collection on the bare and oF_2BPA-modified ZnO surfaces can be seen in **Figure 3**a,c, with the oF2BPA modification leading to a slightly higher open circuit voltage than the bare ZnO (Figure 2). We suspect that decreasing the work function of the contact past the extraction energy levels of the photoactive material may lead to an enhanced charge selectivity and extraction efficiency at the interface.[33–35] Energy level alignment at the oF_2BPA-modified ZnO/BHJ interface likely creates favorable charge transfer conditions resulting in increased V_{oc} and FF with respect to the pristine ZnO ETL-based control device, while pCF_3BPA has the opposite effect.

4. Device Degradation and Enhanced Recovery in the Presence of SAM Modification

In order to evaluate potential changes in the degradation mechanisms introduced by the interfacial modifier layer, devices were stored in air, in the dark, undisturbed for 30 days. After aging, devices were returned to an inert atmosphere (N_2) glove box for electrical testing. The Ag contact was observed by eye to have surface oxidized, but no photo-bleaching of the polymer was observed, as expected for aging devices in the dark. After aging, devices were first tested with no time delay with a 400 nm cutoff filter (see **Figure 4**a) under a 1-sun solar simulator. Devices were then light-soaked under the solar simulator with a 400 nm cutoff filter for 5 min and tested (again with the 400 nm cutoff filter). In the dark, the 400 nm cutoff filter was removed and a 350 nm cutoff filter applied. Devices were light-soaked for 5 minutes and tested, with the 350 nm cutoff filter. The process was repeated for a 335 nm cutoff filter, and finally, with no filter but the glass substrate on which the devices were fabricated (cutoff ≈300 nm). Full *J–V* characteristics obtained from this sequential testing is available in Figure S4 (Supporting Information). Reduction of the cutoff wavelength (past the 380 nm optical band gap of ZnO, Figure S5a,b, Supporting Information) was not observed to play as significant a role as

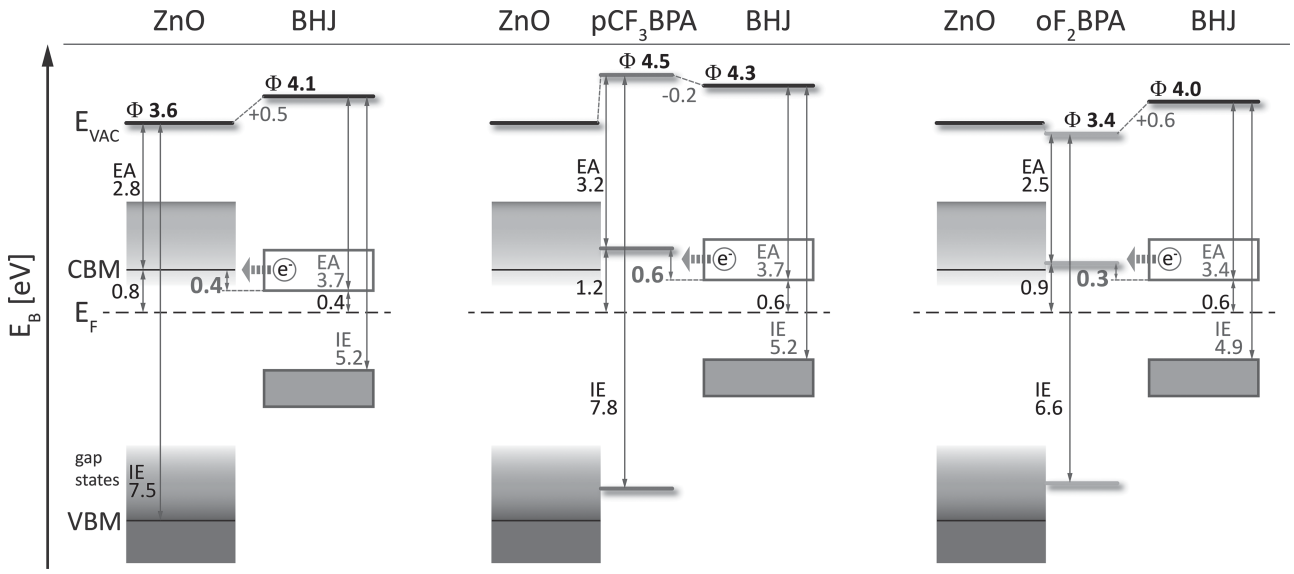

Figure 3. Band diagram of a) bare, b) pCF_3BPA-modified, and c) oF_2BPA-modified ZnO surfaces with adjacent $PC_{71}BM$:PCDTBT BHJ extracted from the spectroscopic measurements of the bare substrates and thin layers of the BHJ. Electron extraction barrier and the magnitude of the interface dipole strongly depend on the surface modification. Bare and oF_2BPA-covered ZnO produce a beneficial scenario for electron transfer across the interface, while the pCF_3BPA-modified surface hinders electrons to move from the LUMO level of the acceptor into the conduction band of the underlying electrode. In (b,c), verification of the change (or no change) of electronic properties in the bulk ZnO is beyond the scope of this work.

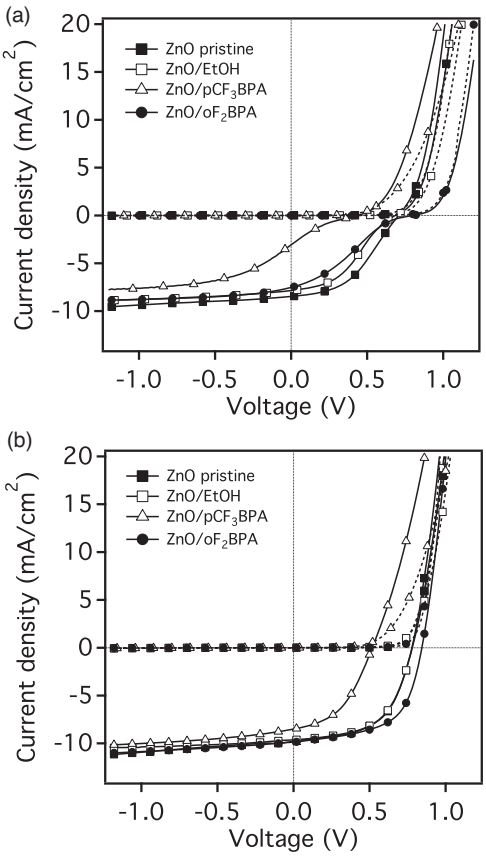

Figure 4. Device characteristics of inverted architecture PCDTBT:$PC_{71}BM$ solar cells using the benzyl phosphonic acids as contact modifiers on the ZnO electron transport layer. After aging in air in the dark for 30 days, devices a) show the development of an S-shape about V_{oc} which b) is reversed after 30 min. full spectrum light-soaking.

the overall time of light exposure (see Figure S5c, Supporting Information). We hypothesize that the parameter important to device recovery is the total energy flux of light absorbed directly into the ZnO material.

Figure 4a,b presents data from the devices with pristine and modified ZnO contacts: *J–V* curves from the 30 day aged devices a) tested with no time delay with the 400 nm cutoff (CO) filter and b) after sequential testing and light-soaking with and without cutoff filter. After 30 days aging, all the devices develop an S-shape *J–V* curve but little to no change in V_{oc}, indicative of a kinetic, rather than energetic, barrier to charge carrier transport/extraction in all devices.[36] After UV light-soaking, the devices recover their as-prepared (pre-aging) diode characteristics, and also show moderate improvement in device performance as seen in **Table 1**.

In order to track changes in performance in the as-prepared devices, and in the aged devices tested with no UV light-soaking as well as after sequential testing and UV light-soaking, the device parameters (*FF*, V_{oc}, PCE) are plotted as a function of UV light exposure time in **Figure 5**a and Supporting Information Figure S6. J_{sc} is roughly independent of aging/light-soaking. Devices with pristine (unmodified) ZnO or ethanol-treated (EtOH) ZnO show gradual improvement of the *FF* in response to increased photon flux and photon energy (Figure 5a). Devices with oF_2BPA-modified ZnO show sharper degradation in initial testing after aging, but also show a strong dependence on light-soaking—namely, faster recovery of the FF, saturation after 350 nm cutoff light-soaking, and a significant improvement in the FF and PCE over as-prepared devices (see Table 1). Devices with pCF_3BPA-modified ZnO show a weaker post-aging recovery of FF, consistent with the kinetic barrier for electron transport/extraction created at the interface in these devices and which necessitates a strong internal electric field and high current densities for efficient carrier transport.

Table 1. Current density-voltage characteristics for Figure 3, glass/ITO/ZnO/(modifier)/PCDTBT:$PC_{71}BM$/MoO_3/Ag inverted architecture organic solar cells.

	J_{sc} [mA cm^{-2}]	FF [%]	V_{oc} [V]	PCE [%]	R_S [Ω cm^{-2}]
As fabricated					
ZnO pristine	10.37	57.9	0.72	4.19	3.7
ZnO/EtOH	10.37	57.9	0.72	4.19	3.6
ZnO/pCF_3BPA	9.34	47.4	0.39	1.67	4.4
ZnO/oF_2BPA	11.02	56.0	0.78	4.38	3.3
Aged 30 days, 400 nm CO filter					
ZnO pristine	8.46	43.5	0.71	3.08	4.3
ZnO/EtOH	7.86	38.3	0.69	2.62	6.4
ZnO/pCF_3BPA	3.06	16.6	0.44	0.32	9.6
ZnO/oF_2BPA	7.53	26.7	0.80	2.13	9.5
Aged 30 days, 300s light-soak					
ZnO pristine	9.77	56.0	0.78	4.35	4.2
ZnO/EtOH	9.65	56.1	0.78	4.38	5.1
ZnO/pCF_3BPA	8.51	44.7	0.52	2.17	7.8
ZnO/oF_2BPA	9.95	60.8	0.85	5.15	2.5

In order to determine the source of the UV light-soaking effect in full device structure, we additionally investigated inverted P3HT:PCBM devices incorporating ZnO contacts modified with alkanethiol self-assembled monolayers (SAMs) (fabrication as detailed in the Experimental Section). After aging of the devices in air in the dark for three days, the samples were returned to the glovebox for measurement. The devices were tested at regular intervals under continuous light-soaking in a standard 1-sun solar simulator with intensity modulated by an OD2.0 neutral density filter, to slow the light-soaking effect. The *J*–*V* characteristics obtained from this sequential testing are available in Figure S7 (Supporting Information). Again, the photovoltaic characteristics were observed to improve dramatically over time with significant improvements in the FF, as seen in Figure 5b. The diode characteristics improve dramatically with light-soaking of the devices, however a substantial decrease in the required light-soaking time is observed for the alkanethiol modified ZnO devices. Here we also observe that the barrier for charge extraction without light soaking is reduced as well, as indicated by the larger initial fill factor for the alkanethiol-modified devices.[24] The work function of the ZnO contact is reduced with the alkanethiol modification similarly to the oF_2BPA case described above, with an increasing change with alkanethiol chain length.[24]

5. Mechanisms of Device Degradation and Enhanced Recovery

Experiments presented in this paper identify the ZnO ETL contact and the ZnO/BHJ and ZnO/modifier/BHJ interfaces to be primary determiners of device performance, i) upon device aging in air and in the dark, and ii) upon performance recovery under UV light-soaking in an inert environment. The degradation and recovery mechanisms may be attributed to effects studied in ZnO from the 1950s[14,37] to the 1980s[13] when ZnO was under investigation as a catalyst material. Researchers established early on that conduction in n-type ZnO occurred through non-stoichiometry of the $Zn_{1+y}O$ material.[14,38] The ratio of excess Zn to O is directly related to the oxide's n-type conductivity. The rate of oxygen chemisorption or desorption from the ZnO material, directly related to electrical conductivity, was shown to be significantly enhanced by UV illumination, with direction of the reaction determined by the balance between the composition of the ZnO material and that of the ambient gases.[37] While chemisorption and desorption of other molecules present in the ambient were isolated and studied,[39,40] oxygen was found to play a key role in modulating the ZnO conductivity. UV illumination, or direct excitation of photogenerated carriers within ZnO, provides additional energy for bond reorganization, enhancing exchange of surface species.

Bonasewicz et al. provide a comprehensive summary of the relationship between surface processes, defect structure, and electrical properties in zinc oxide.[13] They note, for instance, that physisorption of molecular oxygen is observed to occur from 100–250 K, and chemisorption from 300–650 K. Oxygen chemisorption can be described by the charge transfer model:

$$O_2 \rightarrow O_{2,Ads} \xrightarrow{+e} O^-_{2,Ads} \xrightarrow{+e} 2O^-_s \quad (1)$$

where O_2 is gaseous oxygen, the -Ads subscript indicates a chemisorbed molecule or atom, and *e* is an electron. Hence, the presence of photoinduced free charge near the ZnO surface enhances chemisorption. Furthermore, photoinduced carriers may induce photodesorption of the form:

$$ZnO \xrightarrow{h\nu} Zn^+_i + \tfrac{1}{2} O_2 + e \quad (2)$$

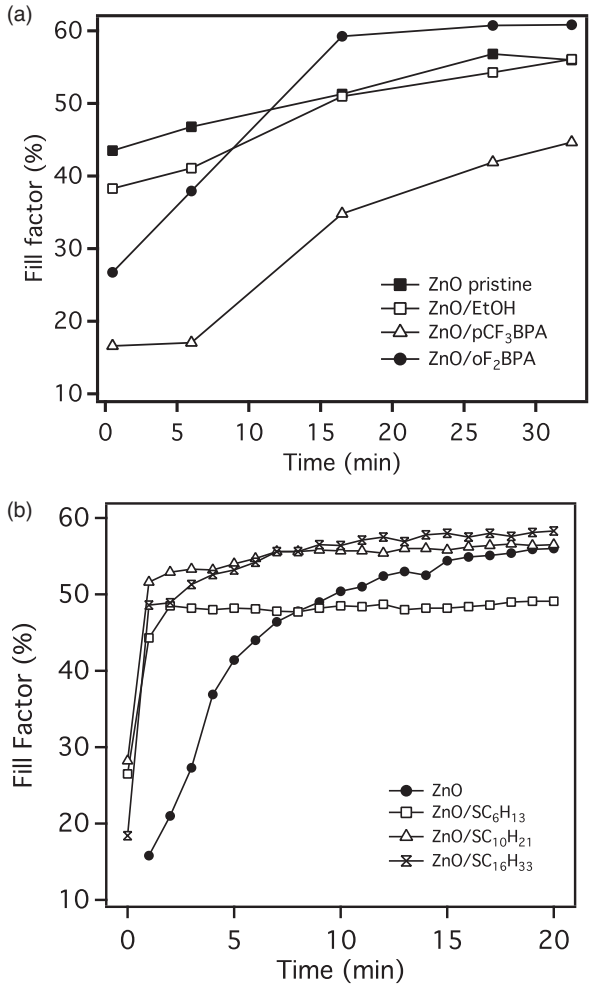

Figure 5. Dependence of FF on illumination time of a) pristine and BPA-modified ZnO ETL-based inverted BHJ PCDTBT:$PC_{71}BM$ solar cells, tested after 30 days aging in the dark, and of b) pristine and thiol-modified ZnO ETL-based inverted BHJ P3HT:PCBM solar cells, tested after 3 days aging in the dark.

where Zn_i^+ is interstitial zinc. We propose that in the inert environment of the glove box, UV light-soaking drives photodesorption of molecular oxygen, thereby increasing the conductivity of the ZnO material and leading to the decrease in series resistance (observed in functioning devices in Supporting Information Figure S8d and Table 1), likely due to an offset between the WF of the contact and the transport level in the photoactive layer.

Furthermore, changing chemical composition of ZnO significantly changes the density of states (DOS) at the valence and conduction band edges, affecting the density of states that carriers see at the BHJ/ZnO interface.[41] Placing a surface modifier at the BHJ/ZnO interface, regardless of the head group, means that the BHJ comes in contact with a much less environmentally variable density of states, as controlled by ZnO's sensitivity to changes in the ambient.

Finally, it is interesting to note that another n-type metal oxide semiconductor, titanium oxide, has been shown to exhibit similar photosorption properties as ZnO.[42,43] In BHJ solar cells incorporating TiO_x as an ETL, a similar S-shape *J–V* curve has been observed to disappear under strong UV irradiation.[44] Kim et al. observed the Fermi level of TiO_x to shift under UV illumination from 4.45 eV to 4.25 eV below the vacuum level, and a concurrent decrease in series resistance and disappearance of the double diode. Other n-type contacts have also shown initial evidence of light-soaking behavior, including Al_2O_3[15] and an n-type small molecule, *N,N′*-bis(3-trimethoxysilylpropyl)-1,6,7,12-tetrachloroperylene-3,4,9,10-tetracarboxyldiimide (Cl_4PSi_2).[45]

6. Kinetic Transport Barrier vs Static Energy Barrier

S-shape current-voltage characteristics have been studied with increasing interest in the field of organic solar cells.[36,46–50] S-shaped *J–V* curves have been attributed, in turn, to reduced surface recombination velocity,[46] to strong interface dipoles,[47] to the accumulation of a non-conductive polymer at the charge extraction interface, to an energy mismatch between HOMOs at the HTL/BHJ interface,[48] and to a mobility imbalance between the donor and acceptor.[36]

In this experiment, we separate two effects often convolved in the study of S-shaped *J–V* characteristics: the development of the characteristic S-shape in the *J–V* curve, and the reduction in open circuit voltage. We modulate the WF and conductivity of the electron transport layer independently, through aging and light-soaking full devices (Figure 3a–c) and through deposition of thin films of benzyl phosphonic acid of increasing thickness on ZnO in Figure 5, respectively. An estimate of the difference in thickness comparing the pCF_3BPA and oF_2BPA layer is derived from the XPS data (see supplementary information). In Figure 5 and **Table 2**, devices composed of pristine and BPA-modified ZnO ETL-based inverted PCDTBT:$PC_{71}BM$ BHJ solar cells are fabricated by varying the solution concentration of the a) pCF_3BPA and b) oF_2BPA modifier. An S-shape *J–V* curve is not present in the solar cell processed from the lowest concentration pCF_3BPA solution, but quickly develops as the solution concentration is increased. Additionally, in response to a small increase in the ETL WF and a larger change in modifier layer thickness and, hence, conductivity (seen in a strong dependence between R_S and BPA deposition conditions), FF and J_{sc} decrease sharply by 70% (45.9% to 13.7%) and 72% (9.97 mA cm^{-2} to 2.77 mA cm^{-2}), respectively, from their initial values, V_{oc} is reduced as well, although to a lesser extent, by 40% (0.53 V to 0.32 V). Increasing the concentration of the pCF_3BPA solution to 10.0 mM results in the formation of a double diode indicating a kinetic barrier to electron extraction. The observed reduction in V_{oc} could be due to the change in work function observed in Figure S9, or to an increase in recombination due to a change in the effective lifetime of carriers (kinetic barrier) in the spatial region near the contact interface as a function of the internal electric field.

As the oF_2BPA layer thickness, and hence the conductivity changes (seen in a strong dependence of R_S on BPA deposition conditions), the device characteristics evolve less strikingly—R_S increases only with the 7.5 mM and 10.0 mM concentrations, leading to a reduction in *FF* (61.3% to 50.2%) and to

Table 2. Current density–voltage characteristics for Figure 4, varying the modifier layer thickness: glass/ITO/ZnO/(modifier)/PCDTBT:$PC_{71}BM$/MoO_3/Ag inverted architecture organic solar cells.

	J_{sc} [mA cm^{-2}]	FF [%]	V_{oc} [V]	PCE [%]	R_S [Ω cm^{-2}]
ZnO pristine	11.13	62.1	0.83	5.75	1.8
ZnO/EtOH	11.21	56.3	0.82	5.20	3.8
ZnO/pCF_3BPA (1.0 mM)	9.97	45.9	0.53	2.43	9.2
ZnO/pCF_3BPA (2.5 mM)	8.75	31.5	0.54	1.49	18.7
ZnO/pCF_3BPA (5.0 mM)	8.02	23.1	0.46	0.86	17.0
ZnO/pCF_3BPA (7.5 mM)	3.29	13.4	0.40	0.18	24.2
ZnO/pCF_3BPA (10.0 mM)	2.77	13.7	0.32	0.12	26.6
ZnO/oF_2BPA (1.0 mM)	10.95	60.2	0.83	5.50	3.5
ZnO/oF_2BPA (2.5 mM)	10.88	58.8	0.83	5.34	3.5
ZnO/oF_2BPA (5.0 mM)	11.48	61.3	0.84	5.93	3.3
ZnO/oF_2BPA (7.5 mM)	11.03	59.9	0.84	5.52	6.2
ZnO/oF_2BPA (10.0 mM)	11.57	50.2	0.80	4.66	11.4

the development of an S-shape, and, to a much lesser extent, a reduction in V_{oc} (0.84 V to 0.80 V). In the case of the oF_2BPA modified contact, changing the concentration of the solution gives no evidence of changing the interface electronic characteristics, suggesting that the Fermi level of the contact is pinned closely below the $PC_{71}BM$ LUMO.

In these experiments, an S-shape develops under two conditions. The first corresponds to aging the ZnO-based solar cell in air (Figure 4a). As this S-shape is completely mitigated by UV light-soaking (Figure 4b), we define the mechanism responsible in this case as reversible. The second condition corresponds to the deposition of thicker non-conductive BPA layers seen in **Figure 6**. Because this S-shape is present in as-fabricated devices, and is relatively unchanged by aging and light-soaking (see Figure 4b, Supporting Information Figure S4e,f), we define this second mechanism as irreversible.

By contrast, the change in WF and interfacial dipole, as controlled by the deposition of benzyl phosphonic acids, is independent of the development of the S-shaped curve. Two Kelvin probe experiments show that the contact WF changes negligibly as a function of benzyl phosphonic acid solution concentration (1.0–10.0 mM) and as a function of time films are aged in air (0–30 days) (Figure S9, Supporting Information). Hence, the development of the S-shape due to BPA solution concentration increases or due to aging the devices in air cannot be primarily attributed to change in contact WF. Of significant note is the small change in V_{oc} due to the change in BPA solution concentration (Figure 6), and due to aging and light-soaking. In contrast, change in contact WF and interfacial dipole due to the deposition of oF_2BPA versus pCF_3BPA on ZnO is observed to directly effect the magnitude of V_{oc}, as observed in Figure 2, relatively independent of FF and J_{sc}.

Hence, we conclude that the development of the S-shaped *J–V* curve can be attributed to the development of a kinetic barrier to carrier transport/charge extraction at the contact. In the present experiment, this kinetic barrier is due to the low-conductivity BPA molecule, and to a reduced conductivity in the ZnO layer for all devices when aged in air. In both cases, the contact becomes unable to extract carriers at a rate commensurate with the rate of photogeneration, leading to a mismatch between the ideal and actual carrier extraction rates at the contact and strongly field-dependent carrier extraction. Conversely, the change in the energy level alignment at the contact interface creates a static energetic barrier, responsible for a change in the "flat-band" potential—but with little to no change to the field-dependent carrier extraction rate. A ZnO UV light-soaking study by Small et al. suggests a similar decoupling of the origins of the S-shape and change in V_{oc}.[48] Future device models of S-shaped *J–V* characteristics should be able to separate the development of the S-shape from change in V_{oc}. Further experiments isolating the role of contact work function, conductivity, and blocking characteristics are ongoing.

7. Conclusion

Poor chemical resistance has prevented, except in two cases,[12,23] work function modification of thin films of ZnO via dipole interface modifiers such as benzyl phosphonic acid, shown to modify the work function of ITO and to modulate the open circuit voltage in full devices.[26,30,31] We confirm that work function modification of the ZnO interface via spin-cast dipole interface modifiers translates into a proportional modulation of the open circuit voltage in BHJ solar cells, as shown in previous work for different electrode materials.[12,26] Spin-casting minimizes exposure of the ZnO to the acidic BPA solution, allowing non-destructive deposition of acid surface modifiers. Deposition of BPAs and alkanethiol SAMs are shown to improve initial device performance and to have a beneficial effect at mitigating the light-soaking effect present after aging in air inverted BHJ devices incorporating ZnO contact layers. Furthermore, we show that ZnO films aged in air show significant increase in series resistance and kinetic barrier to charge extraction. We propose a well-studied mechanism—the exposure of the ZnO

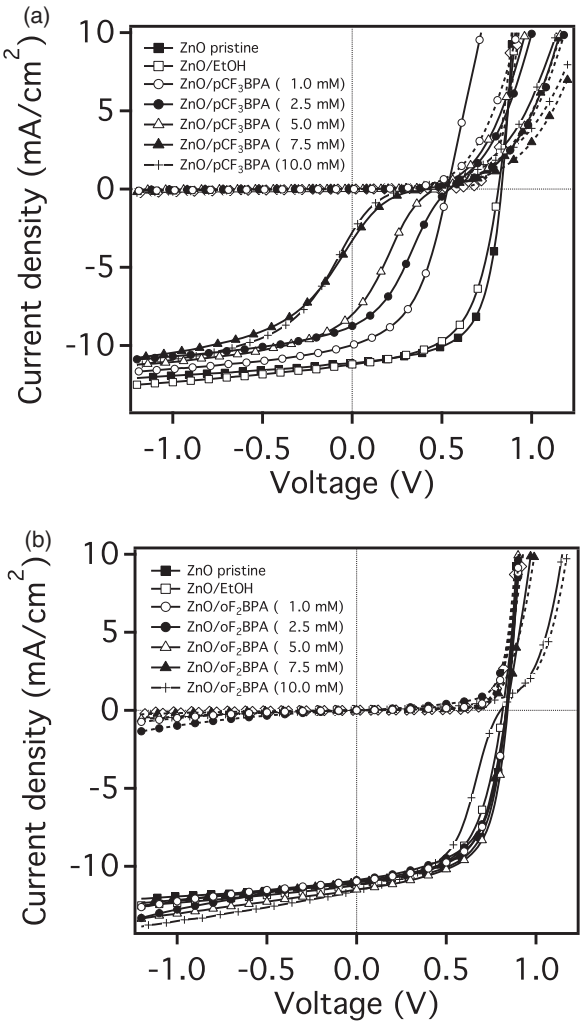

Figure 6. Current–density voltage curves of pristine and BPA-modified ZnO ETL-based inverted PCDTBT:$PC_{71}BM$ BHJ solar cells fabricated by varying the solution concentration of a) pCF_3BPA and b) oF_2BPA modifier.

thin film to molecular oxygen leads to O_2 chemisorption and a reduction in conductivity.

Further, we isolate the effect of a static energetic barrier due to the change in work function from the oF_2BPA and resulting in a decrease in V_{oc}, and of kinetic extraction/transport barriers due to low mobility interface layers or reduced conductivity of the ZnO ETL resulting in the formation of S-shaped *J–V* curves. Future device models of S-shaped *J–V* characteristics should be able to separately control contact work function and conductivity.

8. Experimental Section

Films for electronic characterization and devices are prepared on patterned glass/ITO sourced from Thin Film Devices, Inc., or on glass microscope slides as noted. Thin Film Devices patterned ITO has >84% optical transmission, sheet resistance of ≈10 Ω $\square^{-1}$, thickness of 280 nm, and RMS surface roughness ≈4–5 nm. All substrates are cleaned by sonication in electronic grade acetone and isopropanol for 30 minutes each, then blown dry, placed in clean petri dishes, and set to dry in an oven, T>100 °C, overnight.

For UV-Vis Spectroscopy and Kelvin Probe: Prior to thin film deposition, microscope slide glass or glass/ITO substrates are UV-O_3 (Jelight Company, Inc. Model 42) treated for ≈1 h, and used immediately after removal. ZnO and BPA films are cast as in devices. An HP UV-Visible Chem-Station 8453 is used for UV-Vis spectroscopy. For Kelvin probe, a KPTechnology SKP/SVP/LE 450 system is utilized, calibrated with an Al/Au reference in air.

Device Fabrication: Prior to thin film deposition, glass/ITO substrates are UV-O_3 treated for ≈1 h, and used immediately after removal. ZnO is prepared in an inert environment (N_2) from diethylzinc precursor – 1.1 M in toluene from Sigma Aldrich, additionally stabilized by mixing (1:3) by volume in anhydrous tetrahydrofuran (Sigma Aldrich). ZnO films are spin-cast in air to a thickness 45 nm with variation across the 1" × 1" substrate ±5 nm, or conditions of 7000 RPM for 60 s. Subsequently, films are annealed at 120 °C in air for 20 min. Benzyl phosphonic acids (BPA) are synthesized as previously reported,[30,31] stored in air, and dissolved in ethanol to 1–10 mM concentration. BPA films are formed via spin casting at 2000 RPM for 60 s, and subsequently annealed at 120 °C, 2 min. to promote solvent drying. Films of BPA are too thin to estimate thickness, but the presence of the BPAs is verified via XPS. Samples are subsequently transferred to a nitrogen environment (glove box, O_2, H_2O < 5 ppm) for bulk heterojunction deposition and annealing. PCDTBT (Konarka):$PC_{71}BM$ (Nano-C) (both used as received, mixed 1:4 by weight) are dissolved in 1,2-dichlorobenzene (DCB) : chlorobenzene (CB) (3:1 by volume) (both anhydrous, Sigma Aldrich). Films of 85 nm ± 5 nm (measured by profilometer) are cast by spinning at 4600 RPM, 40 s. Films are annealed at 70 °C, 10 min. Molybdenum oxide (Sigma Aldrich) is deposited via thermal evaporation at 5×10^{-7} Torr at 0.2 Å s^{-1}, to a thickness of 10 nm. Films are then annealed in the glove box at 80 °C, 10 min. The Ag cathode is deposited by thermal evaporation at 1×10^{-7} Torr at 0.5 Å s^{-1}, for a thickness of 100 nm. Devices were aged for 30 days in air in the dark, and tested as-fabricated, as-aged for 30 days with UV-illumination blocked, and under sequential light-soaking under 1 sun illumination. Further, P3HT:PCBM devices incorporating ZnO contacts modified with alkanethiol self-assembled monolayers (SAMs) were fabricated. Hexanethiol (SC_6H_{13}), decanethiol ($SC_{10}H_{21}$), and hexadecanethiol ($SC_{16}H_{33}$) were deposited on the ZnO contact by soaking for 24 h in 1 mM alkanethiol solutions in ethanol at room temperature. After rinsing with ethanol, the active layer (P3HT:PCBM) was spin-cast on the alkanethiol modified ZnO contacts, and devices were completed with MoO_3/Ag contacts. These devices were tested after 3 days aging in the dark in air, and under 1 sun illumination modulated with an OD2.0 neutral density filter to slow the light-soaking effect.

Device Testing: Device testing was carried out under standard 1-sun, AM1.5G test conditions using a solar simulator (quartz halogen lamp with a calibrated mismatch factor of 1.1 compared with the solar spectrum for PCDTBT:$PC_{71}BM$) housed in an inert (N_2) atmosphere. Contact was made to both the ITO and Ag electrodes, from which voltage was sourced and the resulting current was measured. The short-circuit current (J_{sc}) was calculated based on a measured device area of 0.11 cm^2. The series resistance (R_S) was calculated at 1.2 V applied bias.

For Spectroscopy: UPS measurements were performed with He I (21.22 eV) radiation line from a discharge lamp, with a resolution of 0.15 eV, as determined from the width of the Fermi step measured on a clean Au surface. XPS was done at 25 eV pass energy using Al Kα (1486.6 eV) photon line to measure the P 2p, F 1s, C 1s, O 1s, and Zn 2p core levels at an overall resolution of 0.9 eV in order to confirm adsorption of the BPA molecules on the surface. IPES spectra were taken in isochromat mode at a resolution of 0.45 eV, which again was determined from the width of the Fermi step on a sputter clean Au surface.

Acknowledgements

S.R.C. acknowledges funding from the Office of Energy Efficiency and Renewable Energy (EERE) Postdoctoral Research Fellowship through the

SunShot Solar Energy Technologies Program. This work was supported as part of the Center for Interface Science: Solar Electric Materials, an Energy Frontier Research Center funded by the U.S. Department of Energy, Office of Science, Office of Basic Energy Sciences under Award Number DE-SC0001084. The authors acknowledge Mr. Skyler Jackson for work function measurements on ITO.

Received: January 16, 2014
Revised: February 28, 2014
Published online: April 22, 2014

[1] Press release, http://www.heliatek.com/ (accessed January 2014).
[2] J. You, L. Dou, K. Yoshimura, T. Kato, K. Ohya, T. Moriarty, K. Emery, C.-C. Chen, J. Gao, G. Li, Y. Yang, *Nat. Commun.* **2013**, *4*, 1446.
[3] M. A. Green, K. Emery, Y. Hishikawa, W. Warta, E. D. Dunlop, *Prog. Photovoltaics: Res. Appl.* **2013**, *21*, 827.
[4] S. Chen, C. E. Small, C. M. Amb, J. Subbiah, T.-H. Lai, S.-W. Tsang, J. R. Manders, J. R. Reynolds, F. So, *Adv. Energy Mater.* **2012**, *2*, 1333.
[5] W. Li, A. Furlan, K. H. Hendriks, M. M. Wienk, *J. Am. Chem. Soc.* **2013**, *135*, 5529.
[6] Z. He, C. Zhong, S. Su, M. Xu, H. Wu, Y. Cao, *Nat. Photonics* **2012**, *6*, 593.
[7] C. Cabanetos, A. El Labban, J. A. Bartelt, J. D. Douglas, W. R. Mateker, J. M. J. Fréchet, M. D. McGehee, P. M. Beaujuge, *J. Am. Chem. Soc.* **2013**, *135*, 4656.
[8] L. Dou, J. Gao, E. Richard, J. You, C.-C. Chen, K. C. Cha, Y. He, G. Li, Y. Yang, *J. Am. Chem. Soc.* **2012**, *134*, 10071.
[9] M. T. Lloyd, D. C. Olson, P. Lu, E. Fang, D. L. Moore, M. S. White, M. O. Reese, D. S. Ginley, J. W. P. Hsu, *J. Mater. Chem.* **2009**, *19*, 7638.
[10] *Stability and Degradation of Organic and Polymer Solar Cells* (Ed: F. C. Krebs), John Wiley & Sons, Chichester **2012**.
[11] M. T. Lloyd, C. H. Peters, A. Garcia, I. V. Kauvar, J. J. Berry, M. O. Reese, M. D. McGehee, D. S. Ginley, D. C. Olson, *Sol. Energy Mater. Sol. Cells* **2011**, *95*, 1382.
[12] Y. E. Ha, M. Y. Jo, J. Park, Y.-C. Kang, S. I. Yoo, J.-H. Kim, *J. Phys. Chem. C* **2013**, *117*, 2646.
[13] P. Bonasewicz, W. Hirschwald, G. Neumann, *J. Electrochem. Soc.* **1986**, *133*, 2270.
[14] D. A. Melnick, *J. Chem. Phys.* **1957**, *26*, 1136.
[15] Y. Zhou, H. Cheun, W. J. Potscavage Jr, C. Fuentes-Hernandez, S.-J. Kim, B. Kippelen, *J. Mater. Chem.* **2010**, *20*, 6189.
[16] J. Bok Kim, S. Ahn, S. Ju Kang, C. Nuckolls, Y.-L. Loo, *Appl. Phys. Lett.* **2013**, *102*, 103302.
[17] J. Gilot, M. M. Wienk, R. A. J. Janssen, *Adv. Mater.* **2010**, *22*, E67.
[18] C. Donley, D. Dunphy, D. Paine, C. Carter, K. Nebesny, P. Lee, D. Alloway, N. R. Armstrong, *Langmuir* **2002**, *18*, 450.
[19] M. Pourbaix, *Atlas of Electrochemical Equilibria in Aqueous Solution-s*Pergamon Press, Oxford **1966**.
[20] C. F. Baes, R. E. Mesmer, *The hydrolysis of cations*, John Wiley & Sons, New York, **1976**.
[21] C. F. Baes, R. E. Mesmer, *Am. J. Sci.* **1981**, *281*, 935.
[22] W. Gopel, *Prog. Surf. Sci.* **1985**, *20*, 9.
[23] P. J. Hotchkiss, M. Malicki, A. J. Giordano, N. R. Armstrong, S. R. Marder, *J. Mater. Chem.* **2011**, *21*, 3107.
[24] T. C. Monson, M. T. Lloyd, D. C. Olson, Y.-J. Lee, J. W. P. Hsu, *Adv. Mater.* **2008**, *20*, 4755.
[25] H. Li, P. Paramonov, J.-L. Bredas, *J. Mater. Chem.* **2010**, *20*, 2630.
[26] E. L. Ratcliff, A. Garcia, S. A. Paniagua, S. R. Cowan, A. J. Giordano, D. S. Ginley, S. R. Marder, J. J. Berry, D. C. Olson, *Adv. Energy Mater.* **2013**, *3*, 647.
[27] H. Wang, E. D. Gomez, Z. Guan, C. Jaye, M. F. Toney, D. A. Fischer, A. Kahn, Y.-L. Loo, *J. Phys. Chem. C* **2013**, *117*, 20474.
[28] A. Garcia, unpublished.
[29] A. Sharma, B. Kippelen, P. J. Hotchkiss, S. R. Marder, *Appl. Phys. Lett.* **2008**, *93*, 163308.
[30] S. A. Paniagua, P. J. Hotchkiss, S. C. Jones, S. R. Marder, A. Mudalige, F. S. Marrikar, J. E. Pemberton, N. R. Armstrong, *J. Phys. Chem. C* **2008**, *112*, 7809.
[31] P. J. Hotchkiss, H. Li, P. B. Paramonov, S. A. Paniagua, S. C. Jones, N. R. Armstrong, J.-L. Bredas, S. R. Marder, *Adv. Mater.* **2009**, *21*, 4496.
[32] E. L. Ratcliff, J. Meyer, K. X. Steirer, N. R. Armstrong, D. Olson, A. Kahn, *Organ. Electron.* **2012**, *13*, 744.
[33] A. J. Morfa, A. M. Nardes, S. E. Shaheen, N. Kopidakis, J. van de Lagemaat, *Adv. Funct. Mater.* **2011**, *21*, 2580.
[34] C. J. Brabec, A. Cravino, D. Meissner, N. S. Sariciftci, T. Fromherz, M. T. Rispens, L. Sanchez, J. C. Hummelen, *Adv. Funct. Mater.* **2001**, *11*, 374.
[35] V. D. Mihailetchi, P. W. M. Blom, J. C. Hummelen, M. T. Rispens, *J. Appl. Phys.* **2003**, *94*, 6849.
[36] W. Tress, A. Petrich, M. Hummert, M. Hein, K. Leo, M. Riede, *Appl. Phys. Lett.* **2011**, *98*, 063301.
[37] T. I. Barry, F. S. Stone, *Proc. R. Soc. London, Ser. A* **1960**, *255*, 124.
[38] A. Klein, *Transparent conductive zinc oxide* (Eds: K. Ellmer, A. Klein, B. Rech), Springer, New York **2008**.
[39] A. Jones, T. A. Jones, B. Mann, J. G. Firth, *Sens. Actuators* **1984**, *5*, 75.
[40] F. S. Stone, *J. Solid State Chem.* **1975**, *12*, 271.
[41] H. Li, L. K. Schirra, J. Shim, H. Cheun, B. Kippelen, O. L. A. Monti, J.-L. Bredas, *Chem. Mater.* **2012**, *24*, 3044.
[42] D. R. Kennedy, M. Ritchie, J. Mackenzie, *Trans. Faraday Soc.* **1958**, *54*, 119.
[43] S. Fukuzawa, K. M. Sancier, T. Kwan, *J. Catalysis* **1968**, *11*, 364.
[44] J. Kim, G. Kim, Y. Choi, J. Lee, S. H. Park, K. Lee, *J. Appl. Phys.* **2012**, *111*, 114511.
[45] A. W. Hains, H.-Y. Chen, T. H. ReillyIII, B. A. Gregg, *ACS Appl. Mater. Interfaces* **2011**, *3*, 4381.
[46] A. Wagenpfahl, D. Rauh, M. Binder, C. Deibel, V. Dyakonov, *Phys. Rev. B* **2010**, *82*, 115306.
[47] A. Kumar, S. Sista, Y. Yang, *J. Appl. Phys.* **2009**, *105*, 094512.
[48] C. E. Small, S. Chen, J. Subbiah, C. M. Amb, S.-W. Tsang, T.-H. Lai, J. R. Reynolds, F. So, *Nat. Photonics* **2011**, *6*, 115.
[49] C. S. Kim, S. S. Lee, E. D. Gomez, J. B. Kim, Y.-L. Loo, *Appl. Phys. Lett.* **2009**, *94*, 113302.
[50] W. Tress, K. Leo, M. Riede, *Adv. Funct. Mater.* **2011**, *21*, 2140.